Electronic Supplementary Material (ESI) for Journal of Materials Chemistry C.

Supplementary Information

Efficient Perovskite Solar Cells with Negligible Hysteresis Enabled by Sol-Gel Driven Spinel Nickel Cobalt Oxide as Hole Transport Layer

Ju Ho Lee,[§] *Young Wook Noh,* [§] *In Su Jin, Sang Hyun Park*[§] *and Jae Woong Jung*[§]*

[§]Department of Advanced Materials Engineering for Information & Electronics, Kyung Hee University, 1732 Deogyeong-daero, Giheung-gu, Yongin-si, Gyeonggi-do 446-701, Republic of Korea

Table S1. Electrical conductivity of sol-gel driven NiO and NiCo2O4 annealed at different temperatures.

HTL	Annealing temperature (°C)	Sheet resistance (Ω/sq)	Conductivity (S/cm)
NiO	500	$> 10^6$	$> 2.5 \times 10^{-1}$
$NiCo_2O_4$	340	5.27×10^5	4.89×10^{-1}
	400	7.70×10^5	3.25×10^{-1}
	500	8.37×10^5	2.88×10^{-1}

Table S2. Device parameters for *p-i-n* PSCs employing sol-gel driven $NiCo_2O_4$ (340 °C) at different thickness.

Precursor concentration (wt%)	Thickness (nm)	V_{OC} (V)	J_{SC} (mA/cm^2)	*FF*	PCE (%)
0.5	15	0.96	22.73	0.68	14.78
0.75	20	1.05	22.06	0.74	17.18
1	40	0.96	23.10	0.70	15.58

Table S3. Device parameters and hysteresis index (*HI*) for *p-i-n* PSCs employing sol-gel driven $NiCo_2O_4$ (340 °C) at different scan rates and directions.

Scan rate (mV/s)	V_{OC} (V)		J_{SC} (mA/cm^2)		*FF*		PCE (%)		*HI*
	Forward	Reverse	Forward	Reverse	Forward	Reverse	Forward	Reverse	
10	1.06	1.06	22.48	22.51	0.71	0.64	16.92	15.28	0.111
25	1.06	1.06	22.40	22.36	0.72	0.65	17.10	15.41	0.050
50	1.05	1.06	21.96	22.10	0.71	0.72	16.38	16.87	0.027
100	1.04	1.05	22.57	22.55	0.74	0.75	17.37	17.78	0.022
250	1.05	1.06	22.38	22.39	0.75	0.76	17.63	18.08	0.010
500	1.06	1.06	22.53	22.50	0.76	0.76	18.17	18.13	0.009

Table S4. EIS fitting result for the devices with different HTLs under irradiation.

HTL	R1 (Ω)	R2 (Ω)
$NiCo_2O_4$	42	153
NiO	56	252

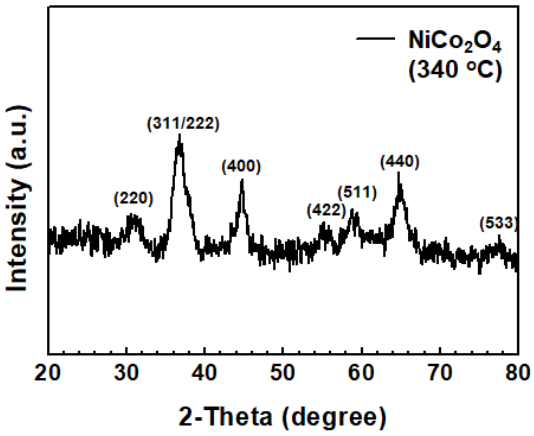

Figure S1. XRD result for $NiCo_2O_4$ thin films annealed at 340 °C.

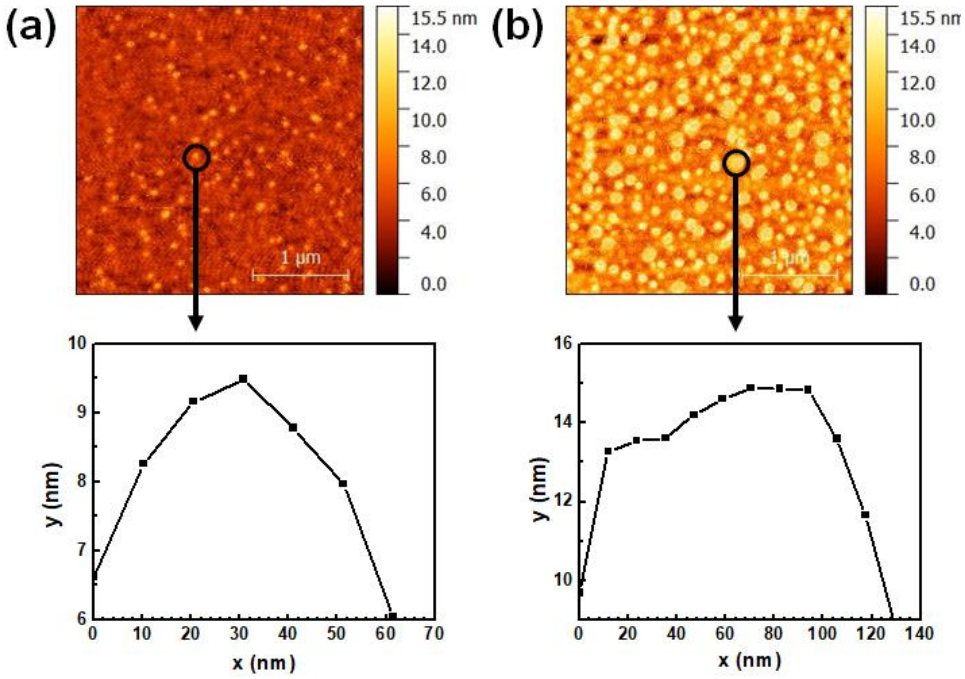

Figure S2. The particle size measurement for NiOx (a) and $NiCo_2O_4$ (b) thin films annealed at 340 °C.

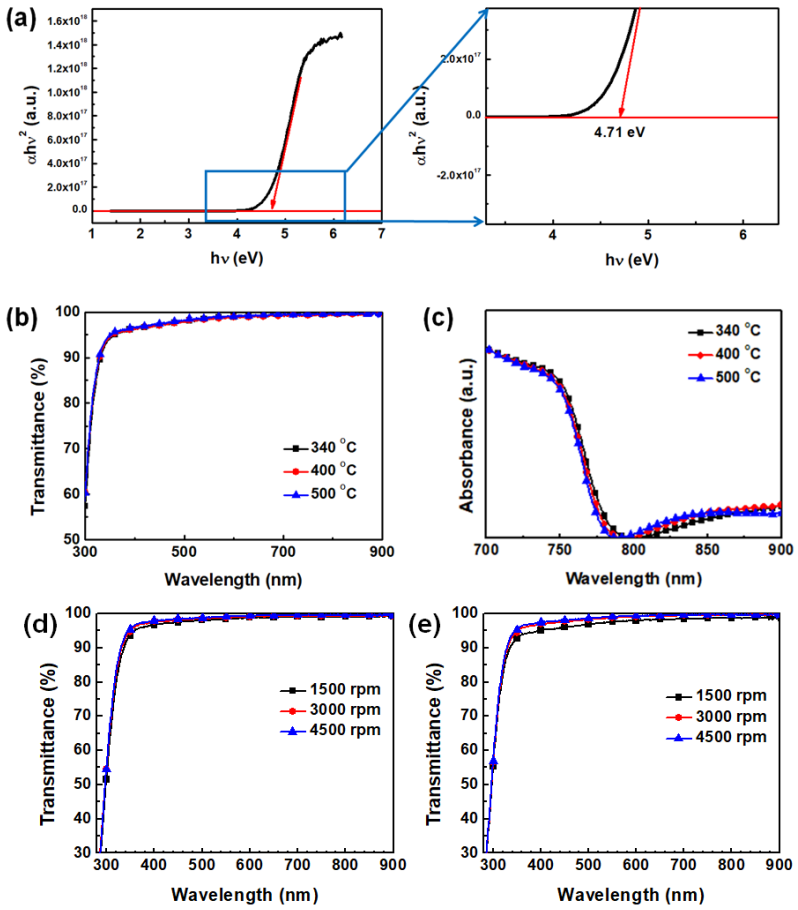

Figure S3. (a) Tauc plot of sol-gel driven $NiCo_2O_4$ thin film, (b) transmittance of sol-gel driven $NiCo_2O_4$ at different temperatures, (c) absorbance of perovskite layer on the sol-gel driven $NiCo_2O_4$ at different temperatures, (d) transmittance of NiO, and (e) $NiCo_2O_4$ thin films with different thickness.

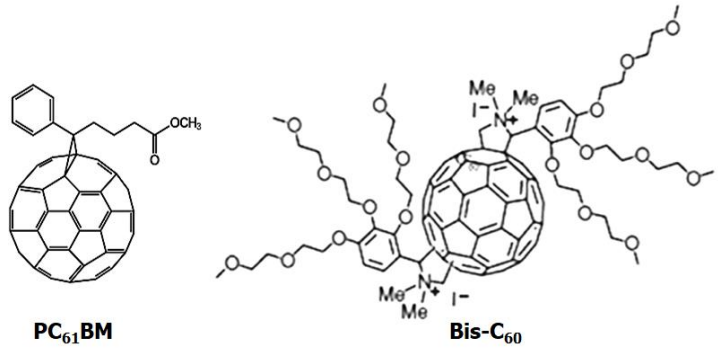

Figure S4. Molecular structure of $PC_{61}BM$ and Bis-C_{60}.

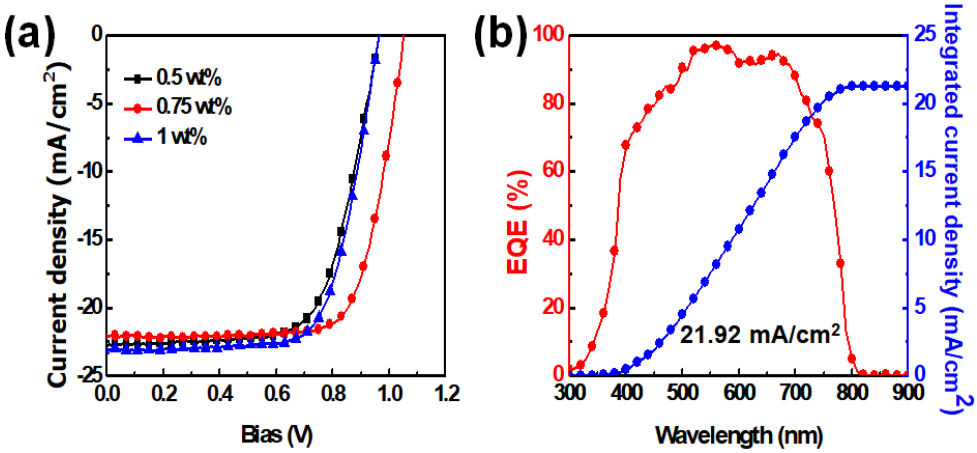

Figure S5. *J–V* curves (a) and EQE spectra for *p-i-n* PSCs employing sol-gel driven $NiCo_2O_4$ (340 ºC) with different concentration of the precursor solution.

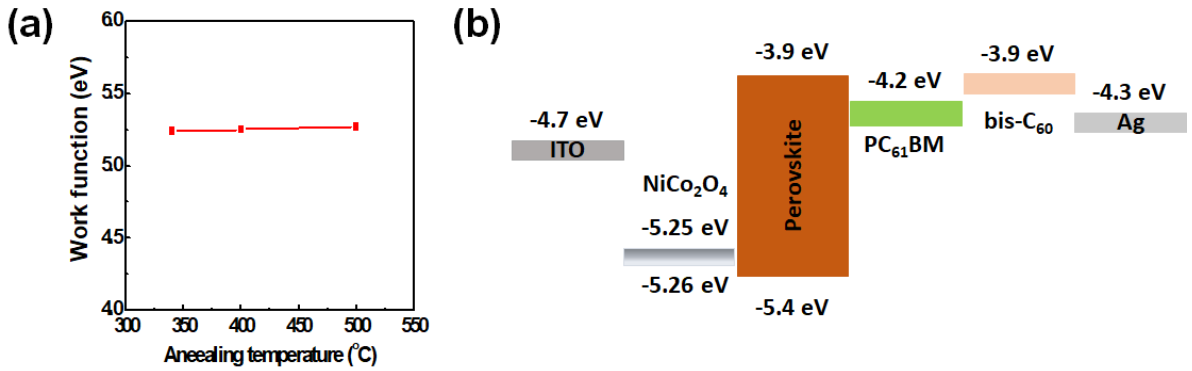

Figure S6. Work function of sol-gel driven $NiCo_2O_4$ thin films prepared at different temperatures (a) and the schematic energy level diagram of the materials used in p-i-n PSCs.

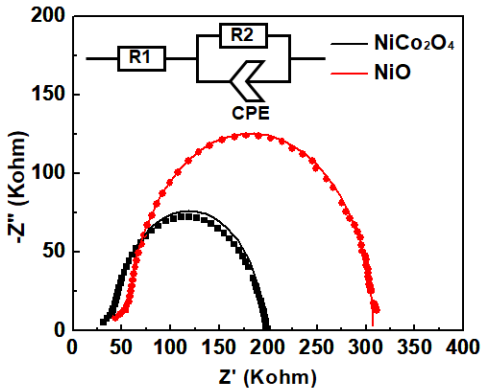

Figure S7. Nyquist plots of the EIS measured on the devices with different HTLs under irradiation.

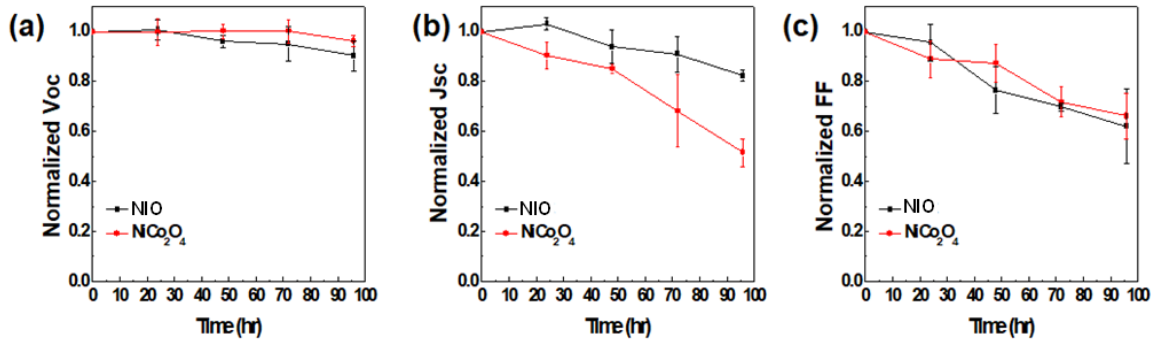

Figure S8. Degradation of V_{OC}, J_{SC}, and *FF* for *p-i-n* PSCs employing sol-gel driven NiO and $NiCo_2O_4$ thin films upon ambient storage with illumination, which was conducted on November 2018.

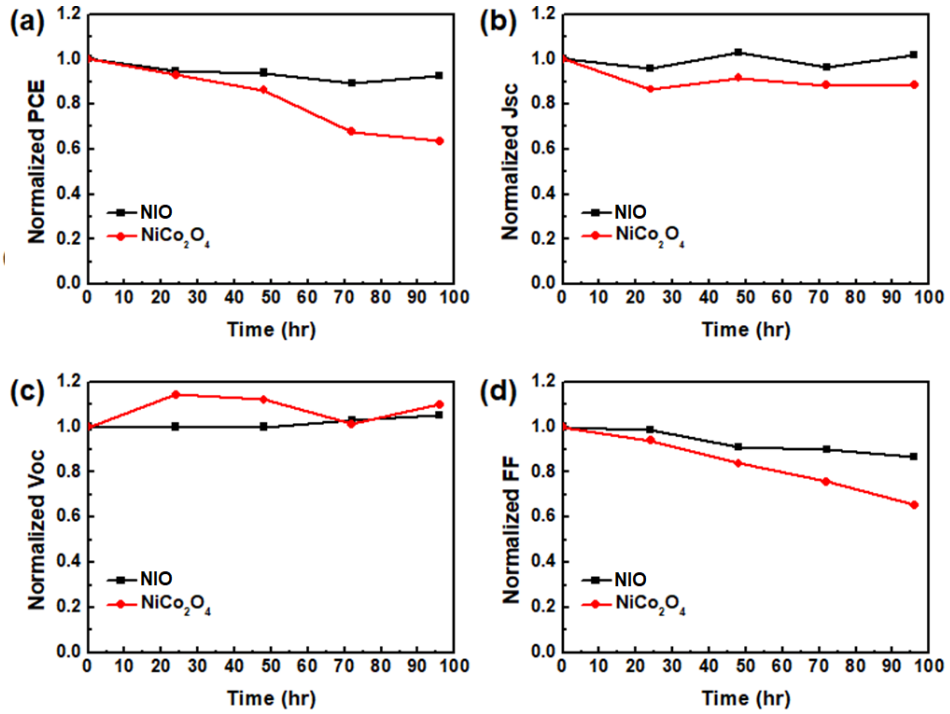

Figure S9. Device stability test for *p-i-n* PSCs employing sol-gel driven NiO and $NiCo_2O_4$ thin films upon ambient storage with illumination that was conducted on March 2019.